

Selective Nanocatalysis of Organic Transformation by Metals: Concepts, Model Systems, and Instruments

Gabor A. Somorjai · Yimin Li

Published online: 11 May 2010
© The Author(s) 2010. This article is published with open access at Springerlink.com

Abstract Monodispersed transition metal (Pt, Rh, Pd) nanoparticles (NP) in the 0.8–15 nm range have been synthesized and are being used to probe catalytic selectivity in multipath organic transformation reactions. For NP systems, the turnover rates and product distributions depend on their size, shape, oxidation states, and their composition in case of bimetallic NP systems. Dendrimer-supported platinum and rhodium NPs of less than 2 nm diameter usually have high oxidation states and can be utilized for catalytic cyclization and hydroformylation reactions which previously were produced only by homogeneous catalysis. Transition metal nanoparticles in metal core (Pt, Co)—inorganic shell (SiO_2) structure exhibit exceptional thermal stability and are well-suited to perform catalytic reactions at high temperatures (>400 °C). Instruments developed in our laboratory permit the atomic and molecular level study of NPs under reaction conditions (SFG, ambient pressure XPS and high pressure STM). These studies indicate continuous restructuring of the metal substrate and the adsorbate molecules, changes of oxidation states with NP size and surface composition variations of bimetallic NPs with changes of reactant molecules. The facile rearrangement of NP catalysts required for catalytic turnover makes nanoparticle systems (heterogeneous, homogeneous and enzyme) excellent catalysts and provides opportunities to develop hybrid heterogeneous-homogeneous, heterogeneous-enzyme and homogeneous-enzyme catalyst systems.

Keywords Catalytic selectivity · Colloid nanoparticles · Oxide metal interfaces

1 Introduction

Stockholm is the cradle of catalysis where, in 1835, J. Berzelius defined the phenomenon when he concluded in his famous paper [1]: “Thus it is certain that substances, both simple and compound, in solid form as well as in solution..., promote the conversion of [chemical compounds]...into other states, without necessarily participating in the process...even if this should occasionally occur.” He defined this phenomenon: “I shall...call it the catalytic power of the substances, and decomposition by means of this power *catalysis*,...” He also envisioned: “Turning with this idea to the chemical processes in living nature, we regard them in a new light... It gives reason to believe that within living plants and animals thousands of catalytic processes are going on between the tissues and fluids, producing a multitude of different chemical compounds...”

In the last century, catalysis developed into one of the most powerful technologies in the petroleum, bulk chemical, fine chemical and pharmaceutical industries [2]. In parallel to developing technologies, our fundamental understanding of catalytic processes has been advancing rapidly by developing model catalytic systems and then studying these model systems using experimental and theoretical techniques at the molecular level [3, 4]. The molecular level knowledge assists the rational design of new catalysts with optimal properties [5].

Activity, selectivity, the resistance to deactivation, and the ability for regeneration are the key macroscopic properties that characterize the usefulness of catalysts. As the concern for environmental protection is continuously

G. A. Somorjai (✉) · Y. Li
Department of Chemistry and Lawrence Berkeley National Laboratory, University of California, Berkeley, CA, USA
e-mail: Somorjai@berkeley.edu

growing in the 21th century, the major challenge we face is to achieve high selectivity without significant degradation of other catalytic properties in order to reduce the cost for product separation and waste disposal [6, 7]. One of the promising strategies in this regard, heterogenization of homogeneous or enzymatic catalysts, aims at combining the superior selectivity of homogeneous and enzymatic catalysts with the recyclability of heterogeneous catalysts [8, 9].

Many industrial heterogeneous catalysts [10, 11] currently in use consist of metal nanoparticles with large variations in size and shape. This variation makes it very difficult to control the distribution of the active sites for different reaction products over the catalyst surfaces. In this paper, we are concerned with how to tune the selectivity of metal-based heterogeneous catalysts using size and shape controlled metal nanoparticles [12, 13]. We start with the concept of the active sites on metal surfaces and its relation to catalytic selectivity (Sect. 2). Then we give a brief introduction to the colloid chemistry controlled nanoparticle synthesis (Sect. 3). Several hydrocarbon conversion reactions using model nanoparticle catalysts are reviewed and the nanoparticle size and shape dependence of the selectivity is discussed (Sect. 4). Section 5 discusses surface science techniques that provide catalyst surface information: the structure, composition, oxidation state, mobility of surface adsorbates, and charge transfer, under reaction conditions and on the molecular scale. Finally, in Sect. 6, we point to future challenges that, we believe, will propel further development of catalysis science.

2 Active Site and Selectivity

The concept of “active sites” in heterogeneous catalysis, introduced by Taylor in 1925, suggested that the concentration of active sites at which the rate-determining step for a specific catalytic reaction occurs is much smaller than the total concentration of available surface sites [14]. For a multiple-path catalytic reaction, the rate-determining steps for different products usually occur on different active sites on the catalyst surface [15–17]. Imagine a catalytic reaction involving a cyclic hydrocarbon reactant (Fig. 1), the scission of the C–C bonds leads to the ring opening product (product 1); while, the dissociation of a C–H bond gives a dehydrogenation product (product 2). The ratio of 1–2 produced at a given surface site are controlled by the relative heights of the Gibbs free energy barriers for two products. At the step sites on platinum surfaces, the scission of C–H bond occurs more readily than that of the C–C bond, which leads to a higher probability for forming the

dehydrogenation product. At the kink sites, the breaking of the C–C bond becomes more facile, and the increase of the ring-opening product is expected. From this simple picture, the selectivity of heterogeneous catalytic reactions is ultimately determined by the relative concentrations of active sites for different reaction pathways. As we will discuss later, this static picture of catalyst surfaces is probably oversimplified since the relative concentrations of active sites may change with time under reaction conditions.

Steady progress has been made in surface science over the last decades in identifying the active sites for different reaction pathways and in controlling the selectivity by tuning the concentrations of active sites on the catalyst surfaces. This progress was partly due to the evolution of model catalytic systems (Fig. 2) and the development of molecular-level surface-science techniques (Table 1). Single crystal metal surfaces provide the model catalysts with well-defined surface structures. The concentrations of terrace, step, and kink sites can be monitored by ultra high vacuum (UHV) techniques such as low energy electron diffraction (LEED). Molecular beam and temperature programmed desorption studies of elementary reaction

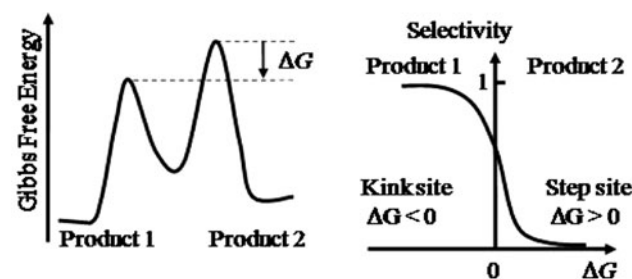
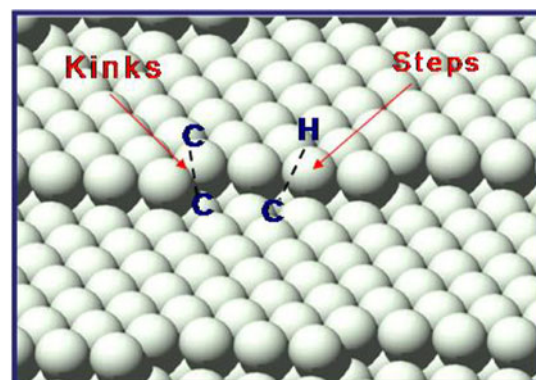


Fig. 1 The upper panel: the model kinked Pt surface (the upper panel). The C–C bond and C–H bond are dissociated at the kink and step site, respectively. The lower left panel: the schematic free energy potential surface for two-pathway reaction. Product 1 is formed by breaking the C–C bond, and Product 2 is formed by breaking the C–H bond. The activation barrier for product 1 is lowered at the kink site, which leads to the difference in selectivity between the step and kink site as shown in the lower right panel

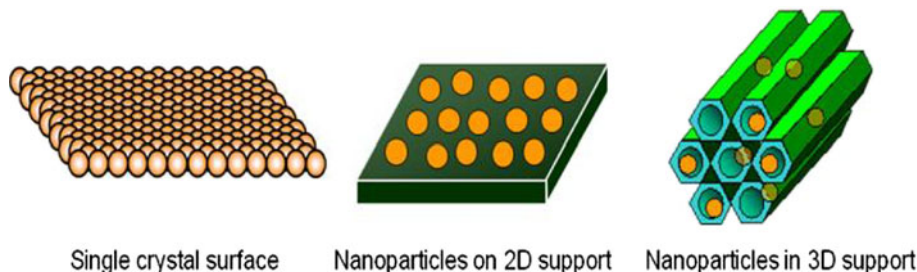


Fig. 2 Three types of the model catalysts developed to study the active sites on the catalyst surfaces. Surface structure of single crystal catalysts is relatively easy to control and to characterize by available surface science techniques. The selectivity studies over the single crystal surfaces provide information about the active sites, which can serve as references for nanoparticle catalyst studies. By dispersing the size and shape controlled nanoparticles onto 2D supports, many of

surface science techniques are still applicable for characterizing the surface of these nanoparticles. Nanoparticle size and shape effects on catalytic selectivity can be studied systematically. The effect of strong metal support interaction can also be investigated. Loading nanoparticles onto high-surface-area 3D supports produces systems similar to those used in industry and enables the selectivity studies under reaction conditions practiced in chemical technologies

Table 1 Ex-situ and in situ surface science techniques for characterizing the model catalysts

Ex-situ characterization

Transmission electron microscopy (TEM)
X-ray diffraction (XRD)
Diffuse reflectance UV–Vis spectroscopy
X-ray photoelectron spectroscopy (XPS)
Scanning electron microscopy (SEM)
Chemisorption, physisorption
Small angle X-ray scattering (SAXS)
Energy dispersive X-ray analysis (EDX)
Thermogravimetric analysis (TGA)
Temperature programmed oxidation (TPO)
Inductively coupled plasma–optical emission spectroscopy (ICP–OES)
Spectroscopies and microscopy for in situ characterization
High-pressure scanning tunneling microscopy (HP-STM)
Sum frequency generation spectroscopy (SFG)
Ambient-pressure X-ray photoelectron spectroscopy (APXPS)
Diffuse reflectance infrared spectroscopy (DRIFTS)
UV-Raman and surface enhanced raman spectroscopy (SERS)
Transmission electron microscopy (TEM)
Tapered element oscillating microbalance (TEOM)
Thermogravimetric analysis (TGA)
UV–Vis diffuse reflectance spectroscopy
X-ray diffraction (XRD)
Small-angle/wide-angle X-ray scattering (SAXS-WAXS)
Near-edge X-ray absorption fine structure (NEXAFS)
Extended X-ray absorption fine structure (EXAFS)

steps: chemisorption, desorption, and activation of chemical bonds on different crystal surfaces help identifying the active sites in selective reactions [3].

The development of high pressure reaction cells enabled the measurements of reaction turnover rates under realistic

reaction conditions on the well-defined crystal surfaces (Fig. 3a). It was found that the selectivity of many catalytic reactions, for example, the conversion of *n*-hexane on platinum surfaces (Fig. 3b), is highly sensitive to surface structure [18]. The dehydrocyclization of alkanes to aromatic hydrocarbons are more facile on the close-packed Pt(111) surface than on the open (100) surface. The isobutane isomerization to *n*-butane occurs more readily on the Pt(100) and the stepped Pt(13,1,1) surfaces than on the loose-packed Pt(111) surface or the kinked Pt(10,8,7) surface. Hydrogenolysis rates of isobutene are maximized on the surface with high concentration of kink sites.

There are several unique properties of surface structures of solids with different chemical bonds. The surfaces reconstruct when clean. Examples of these are shown in Fig. 4a. When molecules adsorb and form strong chemical bonds with the surface atoms, the substrate can restructure again along with the restructuring of adsorbed molecules as shown in Fig. 4b. Since the active sites on the surface are covered with adsorbates, the reactions are low probability events and the turnover frequency is negligible at low pressures. For example, the C–H dissociation of methane on Pt (111) has a probability as low as $\sim 1 \times 10^{-8}$ at 300 K. After reaction of 1 Torr of methane with Pt(111) for 60 s at 300 K, the sum-frequency generation spectrum shows adsorbed methyl (CH_3) as a broad peak at 2880 cm^{-1} . If the same reaction is performed at 10 Torr of methane, a sharper peak at 2880 cm^{-1} indicates the formation of ethyldyne by coupling adsorbed CH_3 groups and C atoms on the surface [19]. The dramatic effect of reaction pressure on the selectivity have been observed in the cyclohexene hydrogenation and dehydrogenation reaction over the stepped Pt(223) surface with cyclohexene and hydrogen partial pressure ratio fixed at 1/10 [20]. As the total pressure of reactants increases from 10^{-4} Torr to above 1 Torr, the reaction changes from producing benzene

Fig. 3 **a** High pressure reactor for catalytic turnover measurement at high pressures. The small-surface-area (approximately 1 cm^2) is placed in the middle of the chamber which can be evacuated to 10^{-9} Torr (the upper panel of **a**). The surface can be characterized by UHV techniques such as LEED and Auger electron spectroscopy (AES). Then the lower part of the high pressure isolation cell is lifted to enclose the sample (the lower panel of **a**). The pressure isolation cell is connected to a gas chromatograph for the reaction turnover measurements under high pressure conditions. **b** Surface structure sensitivity of *n*-hexane and isobutane conversion observed under high pressure conditions

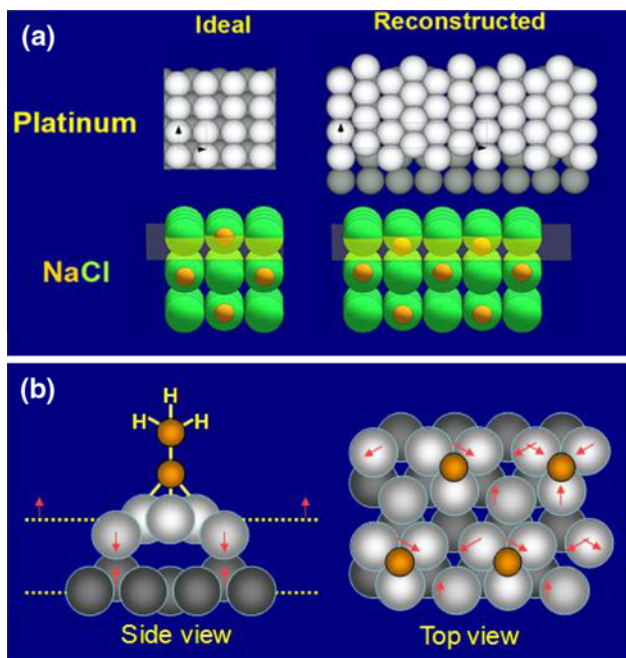
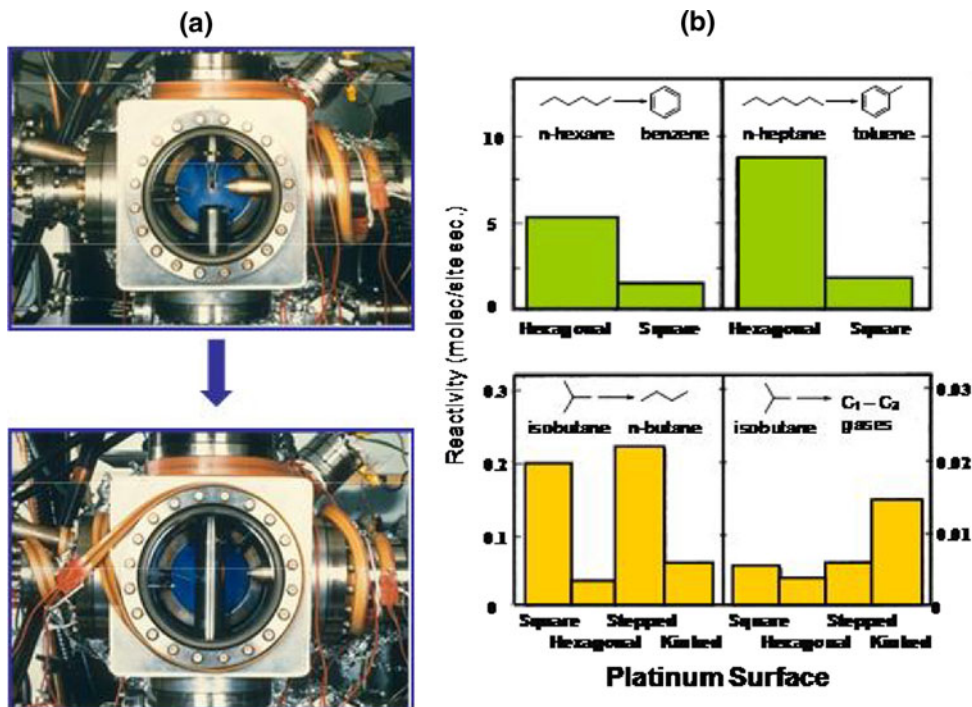


Fig. 4 **a** The reconstructions of clean crystal surfaces. **b** The chemisorption-induced reconstruction of the Pt(111) surface by the ethylene adsorption at the room temperature

exclusively to cyclohexane as predominant product. The complexities of catalysis under high temperatures and high pressures highlight the necessity to develop *in situ* techniques for monitoring active sites and reaction intermediates under reaction conditions which we will discuss more in details later.

The industrial catalysts are usually in the form of metal nanoparticles supported on oxides. These catalysts were developed by empirical trial and error. The metal nanoparticles in these catalysts have a wide size and shape distribution, so it is generally difficult to control the concentrations of active sites on the catalyst surfaces. A successful example of controlling active sites is found in the Fe/aluminum oxide catalysts. The restructuring process of iron induced by water vapor and the presence of aluminum oxide produces an active and stable Fe(111) phase on the support [21, 22].

With the rapid advance in the nanoparticle synthesis in the last decade, the size and shape controlled metal nanoparticles can now be produced routinely [23–25]. These nanoparticles can be dispersed on a 2D support by the Langmuir-Blogett technique, or loaded in 3D oxide support to form model catalyst systems (Fig. 2). By performing turnover measurements on these model catalysts, the size and shape dependence of the selectivity can be studied in detail. Taking advantage of the uniformity of active sites on the size and shape controlled nanoparticle catalysts, the knowledge of active sites obtained from the single crystal studies may be utilized to engineer new generations of nanoparticle catalysts with high selectivity.

3 Synthesis and Characterization of Size and Shape Controlled Nanoparticles

Advances in nanoscience have made it possible to fabricate metal nanoparticles of size in the range of 1–10 nm. The

Fig. 5 The size and shape controlled Pt nanoparticles prepared by the colloid-chemistry controlled method

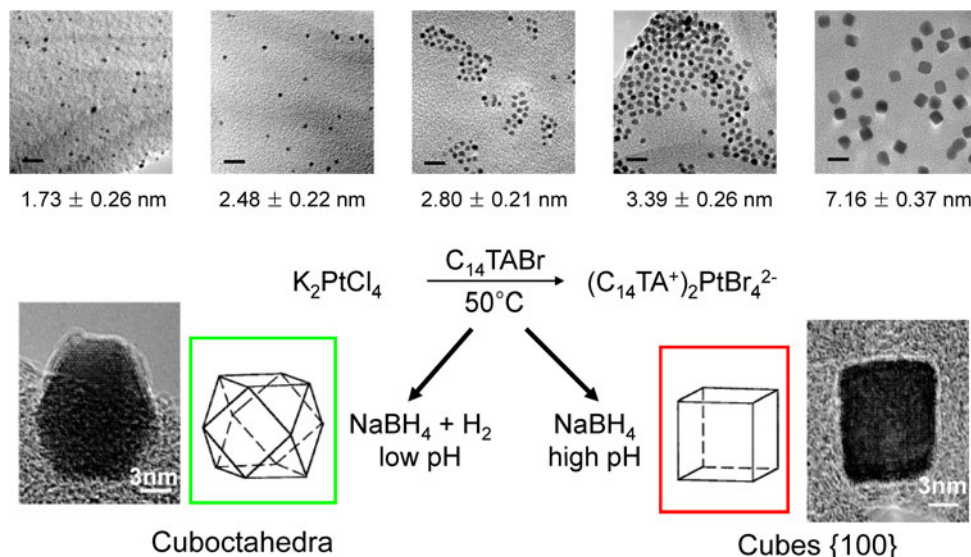
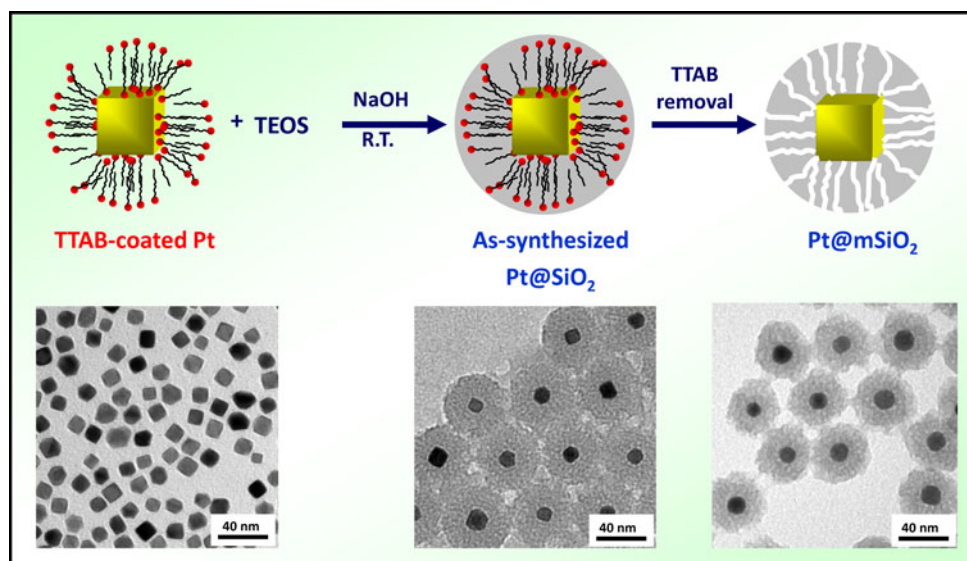


Fig. 6 The Pt nanoparticles coated individually by a silica shell (core–shell structures)



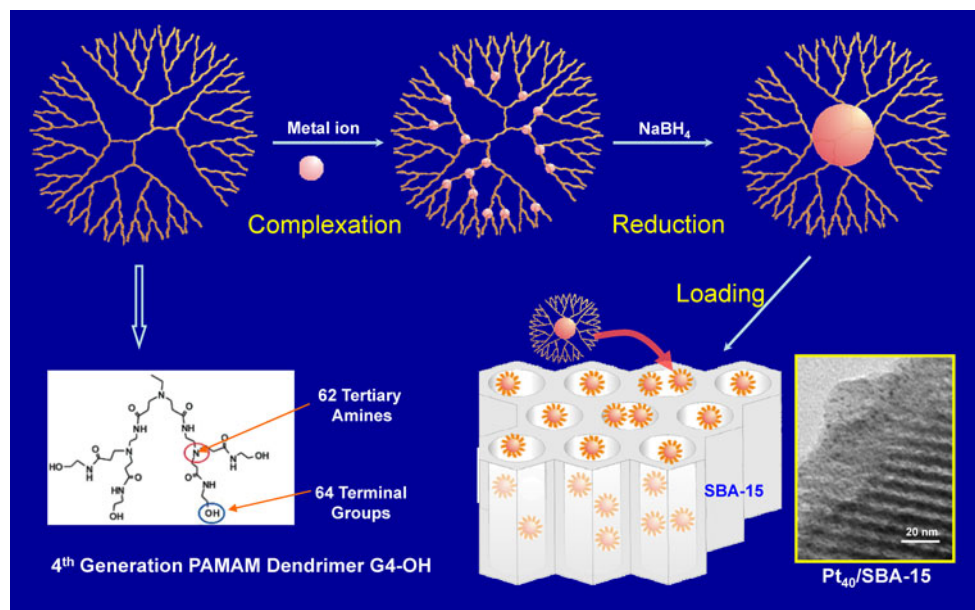
colloid chemistry controlled synthesis has been proved to be the most versatile way of synthesizing the size and shape controlled metal nanoparticles [12, 24]. In this synthesis, a mixture of metal salt and a surfactant agent is reduced by a reduce agent at the appropriate temperature to form nanoparticles coated with a polymer surfactant layer. The size of nanoparticles is controlled mainly by the concentration of the metal salt [26]. The desired shape of nanoparticles can be achieved by adjusting the pH of the mixture, or by adding ions such as Ag^+ and Br^- to the reaction mixture. An example of size and shape controlled Pt nanoparticles [27] is shown in Fig. 5. In this example, the size of nanoparticles is about 1.7–7.2 nm. The surface of the cuboctahedral particles consists of a mixture of (111) and (100) facets. The cubic particles expose only (100) facets.

If one starts with a mixture of two metal salts, it is possible to fabricate bimetallic nanoparticles using the

same approach [28]. In order to keep the monodispersed nanoparticles from aggregation under harsh catalytic reaction conditions, attempts have been made to coat individual nanoparticles with a thermal stable oxide shell. A successful example [29] is shown in Fig. 6. Compared to the uncoated nanoparticles, these cubic Pt nanoparticles coated with the silica shell show exceptional thermal stability during CO oxidation reaction.

Recently, small clusters of dendrimer-encapsulated metal nanoparticles are being explored as ultrafine catalysts [30–32]. The well-defined structure of the dendrimer makes possible the synthesis of ~1 nm nanoparticles. For polyamidoamine dendrimers (Fig. 7), the number of internal amine functional groups, which act as ligands to bind with metal ions, is determined by the dendrimer generation. The metal ions anchored in each dendrimer were reduced and formed a nanoparticle. The dendrimer

Fig. 7 The scheme for synthesizing metal nanoparticles with size of ~1 nm by the dendrimer templating strategy



supplied not only internal cavities for nanoparticle growth upon reduction, but also a shell to prevent aggregation of the as-grown nanoparticles. By changing the metal ion to dendrimer concentration ratio, nanoparticles around 1 nm in diameter can be synthesized with narrow size distribution. The same strategy can be used to synthesize the ultrafine bimetallic nanoparticles.

4 Selectivity of Size and Shape Controlled Nanoparticle Catalysts

In our laboratory, a range of hydrocarbon conversion reactions (Scheme 1) have been studied using size and shape controlled nanoparticle catalysts [33–37]. Attempts have been made to establish correlations between the size and shape of the nanoparticles and the selectivity of these reactions. Ideally, selectivity behavior for a given reaction over different single crystal surfaces should be manifested in the reaction over the shape controlled nanoparticle catalysts. Benzene hydrogenation over the Pt shape controlled nanoparticles is an example which exhibits similar selectivity behavior to that observed on single crystal surface [33]. The two hydrogenation products of this reaction are cyclohexene and cyclohexane. Over the single crystal Pt(111) surface, both products are formed; while, only cyclohexene is formed on the Pt(100) as shown in Fig. 8a. Over the cuboctahedral nanoparticles which have a mixture of (111) and (100) facets, both products are observed, but only cyclohexene is formed on the (100) facets of the cubic nanoparticles as expected (Fig. 8b). This example

demonstrates the control of active sites for selectivity by the nanoscience approach.

4.1 Pyrrole Hydrogenation

Significant size and shape dependence of selectivity was observed during the pyrrole hydrogenation reaction over Pt catalysts [35, 37]. The pyrrole hydrogenation to pyrrolidine is followed by ring opening to *n*-butylamine, and the scission of the N–C bond to form butane and ammonia. Figure 9 shows the *n*-butylamine formation is more facile over larger Pt nanoparticles. The pyrrolidine formation occurs more easily on the smaller Pt nanoparticles. The change of the selectivity becomes significant as the size of nanoparticles is reduced below about 2 nm.

The selectivity of this reaction was also studied over polyhedral and cubic nanoparticles with size of 5 nm (Fig. 10). At about 380 K, the reaction yields about 70% *n*-butylamine and 30% pyrrolidine over the polyhedral nanoparticles in contrast to exclusive *n*-butylamine formation (>90%) over the cubic nanoparticles. As the reaction temperature increases from 380 to 415 K, the *n*-butylamine formation over the polyhedral nanoparticles increases gradually and eventually reaches above 90% at the expense of pyrrolidine formation. Virtually, no selectivity change over the cubic nanoparticles was observed in this temperature range. The turnover rates of this reaction are in order of 0.01 s⁻¹, which has been explained by *n*-butylamine product poisoning. The surface intermediates of this reaction on the Pt surfaces are bonded to the surface through N atom. The N of *n*-butylamine is more electron-rich than other

Scheme 1 Several multipath hydrocarbon conversion reactions for selectivity studies on the model nanoparticle catalysts

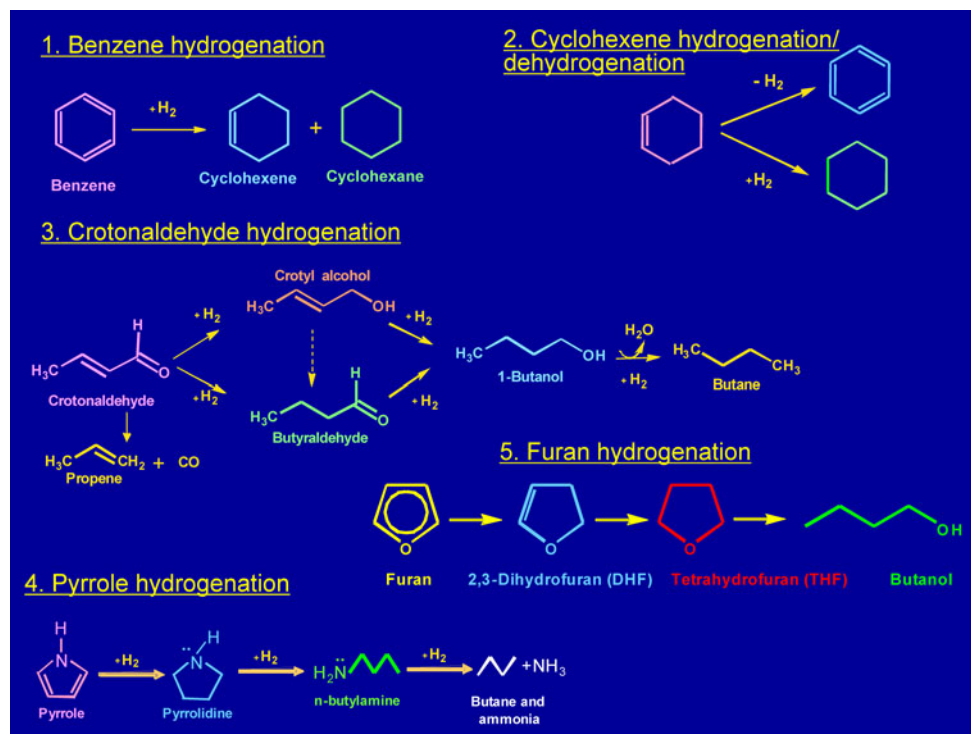
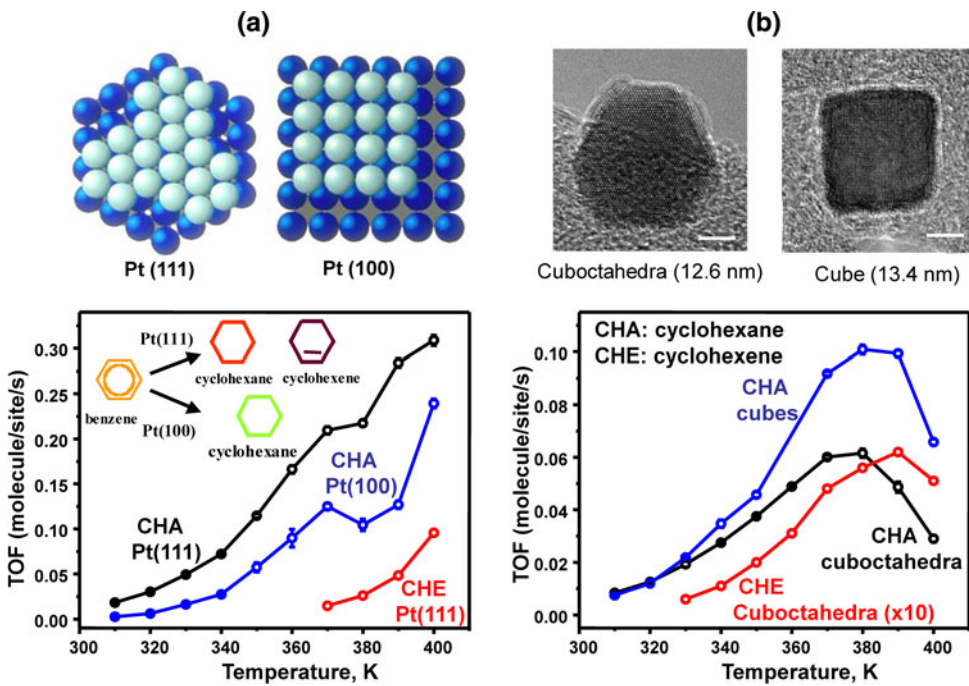


Fig. 8 Comparison of the selectivity of benzene hydrogenation over **a** the single crystal surfaces and **b** the shape controlled nanoparticle catalysts



intermediates such as pyrrolidine or pyrroline and thus can form stronger bonds with the surface and consequently inhibit turnover. Moreover, it is indicated by the SFG results (see next section) that the *n*-butylamine is bonded more strongly to the Pt(100) surface than to the Pt(111) surface. The dominant product of *n*-butylamine on the cubic Pt

nano particles could be explained by the high coverage of *n*-butylamine on the Pt(100) surface, which limits the active sites for the adsorption of pyrrole and the turnover to pyrrolidine. This example brings up another important factor that may affect catalytic selectivity, i.e., the blocking of active sites by strongly adsorbed reaction intermediates.

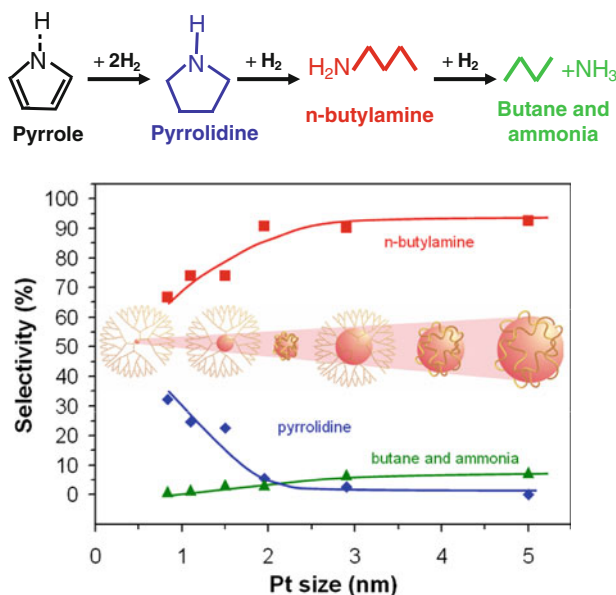


Fig. 9 The nanoparticle size dependence of the selectivity of pyrrole hydrogenation under the reaction condition: 4 Torr pyrrole, 400 Torr H₂, 413 K

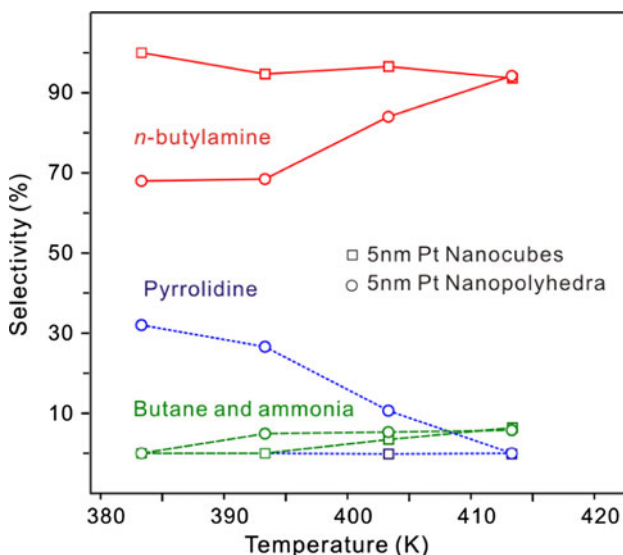


Fig. 10 The nanoparticle shape dependence of the selectivity of pyrrole hydrogenation under the conditions: 4 Torr pyrrole, 400 Torr H₂

4.2 Furan Hydrogenation

More recently, furan hydrogenation has been performed over nanoparticles with different sizes [38]. Three products: 2,3-dihydrofuran (DHF), tetrahydrofuran (THF), and butanol, can be detected from reacting 10 Torr furan with 100 Torr hydrogen, at 363 K. As the nanoparticle size decreases, the formation of the partially hydrogenated

ring product, DHF, increases, and the fully hydrogenated ring product, THF, decreases slightly, while the ring opening product butanol decreases dramatically (Fig. 11). The decrease of the ring opening product with the size reduction is similar to that observed in the pyrrole hydrogenation. However, there seems no dominant surface intermediate species in this case as suggested by *in situ* SFG studies, so a more complicated mechanism is indicated to account for the size induced selectivity change in this reaction.

4.3 Cyclization Reactions in Solution Phase

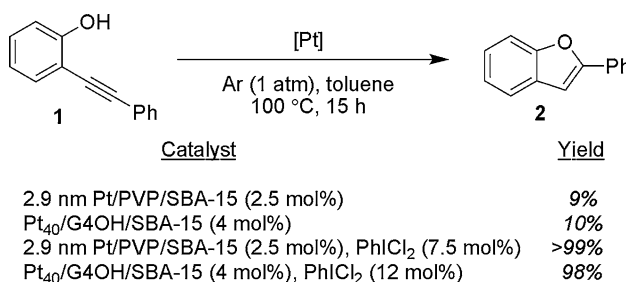
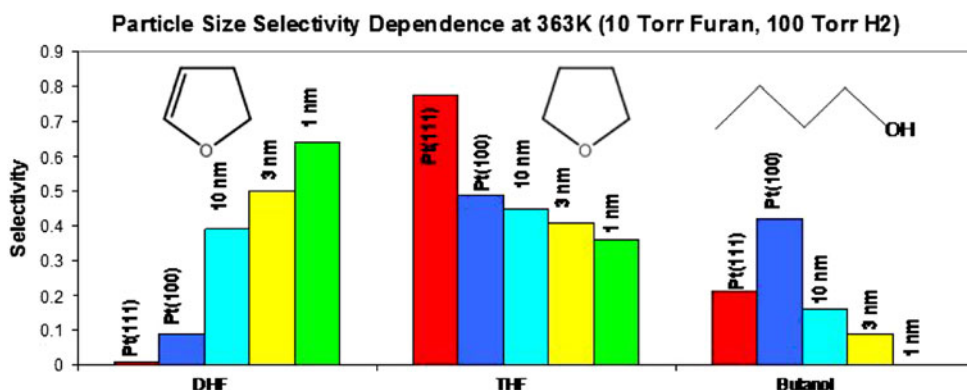
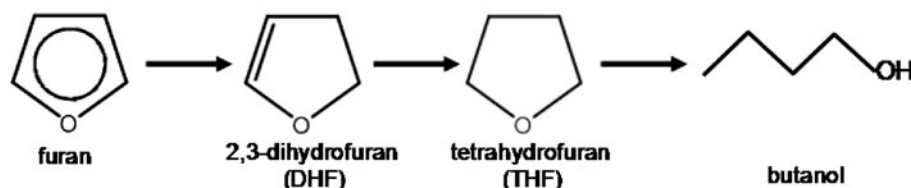
Pt nanoparticles supported on mesoporous silica SBA-15 have been successfully applied to catalyze the cyclization of phenyl alkyne in solution phase shown in Scheme 2 [39]. This reaction is conventionally carried out by the homogeneous catalyst, PtCl₂. The use of heterogeneous approach improves recyclability of the catalyst which is a major advantage.

In the homogeneous catalysis process, the electrophilic Pt⁺² is the active site for activating the π -bond in phenyl alkyne. In order for the heterogeneous catalyst to achieve the same selectivity as the homogeneous catalyst, the heterogeneous Pt catalyst must be activated by treatment with the mild oxidant PhICl₂. The resulting electrophilic Pt catalyst is capable to selectively catalyze a series of cyclization reactions in which π -bond activation is essential (Scheme 3). A number of leaching tests have been performed in order to verify the heterogeneity of the catalytic process (see Ref. [38] for more detail).

5 In situ Surface Science Techniques for Monitoring Active Sites on Catalyst Surfaces

Studies by surface science techniques under the low pressure and low temperature conditions are good at proposing the possible active sites responsible for different products [16]. However, these active sites are not necessarily thermodynamically and/or chemically stable under realistic reaction conditions. As we have discussed in previous sections, these active sites may be reconstructed at high temperatures, or blocked by strongly adsorbed surface intermediates under high pressures. Thus, the grand challenge at present is to develop *in situ* surface science techniques which are capable to identify the active sites under realistic reaction conditions. Several major *in situ* techniques for heterogeneous catalysis studies are listed in Table 1. Here, four techniques developed at Berkeley will be discussed.

Fig. 11 The nanoparticle size dependence of furan hydrogenation. The selectivities over surfaces Pt(111) and Pt(100) single crystal surfaces are also shown for comparison

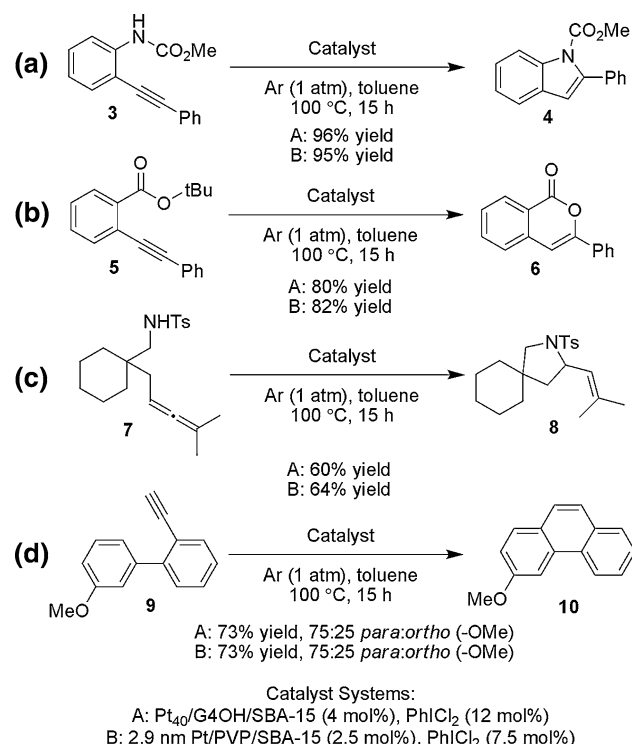


Scheme 2 The cyclization of phenyl alkyne catalyzed by Pt nanoparticles in the solution phase

5.1 Sum-Frequency Generation (SFG) Vibrational Spectroscopy

SFG Vibrational Spectroscopy [40, 41] is a nonlinear spectroscopy technique in which two high-energy pulsed laser beams are overlapped spatially and temporally on an interface of interest. Due to the properties of the nonlinear susceptibility tensor, media with inversion symmetry such as isotropic gases or bulk metal crystals cannot generate a SFG signal. Thus, the entire signal is generated at the interface. The infrared visible SFG process (Fig. 12) can be thought of as infrared and visible excitations followed by an antistokes Raman relaxation emission at the sum of the two incoming frequencies. This technique has been applied in our laboratory to many catalytic reactions over single crystal and nanoparticle model catalysts at high pressure [42, 43].

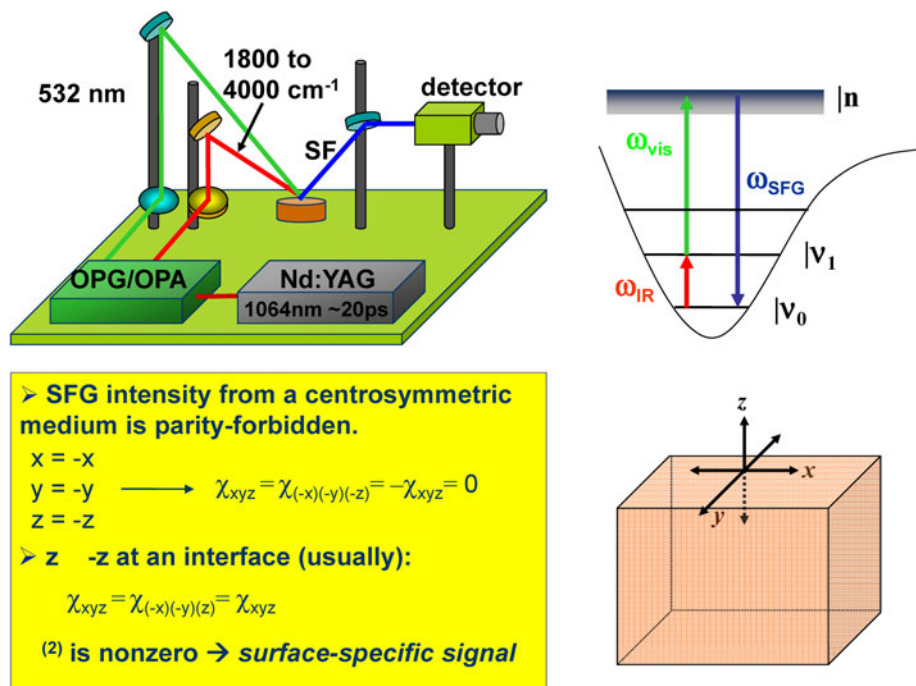
This technique helps us determine the major reaction intermediates on the catalyst surfaces and understand the competition between intermediates for active sites. For



Scheme 3 A series of cyclization reactions catalyzed by the PhICl₂-activated Pt nanoparticles

example, Fig. 13 shows the SFG spectra of the Pt(111) and Pt(100) surfaces during the pyrrole hydrogenation [37, 44]. In these spectra, the C-H_x vibrational modes below about 3000 cm⁻¹ can be attributed to the adsorbed *n*-butylamine. On the Pt(111) surface, the C–H aromatic stretching mode at 3105 cm⁻¹ indicates that an intact aromatic ring is

Fig. 12 Scheme for the experimental setup and the operating principle of sum frequency generation (SFG) vibrational spectroscopy



adsorbed on the surface at 298 K. Thus, at 298 K, *n*-butylamine and certain aromatic species are coadsorbed on the Pt(111) surface. The disappearance of the aromatic stretching mode on the Pt(111) surface at 363 K indicates *n*-butylamine is bonded more strongly to the surface than the aromatic species. In contrast, the lack of the aromatic stretching mode on the Pt(100) surface at 298 K suggests that *n*-butylamine is bonded more strongly to the Pt(100) surface than to the Pt(111) surface and blocks the sites for the adsorption of the aromatic species on the Pt(100) surface. These findings can be applied to understand the shape dependence of selectivity over the different nanoparticle catalyst (Fig. 10). Considering that the polyhedral nanoparticles expose a mixture of the (111) and (100) surface, while that the cubic nanoparticles have mostly (100) surfaces, we expect more aromatic species coadsorbed with *n*-butylamine on the polyhedral nanoparticle surfaces and consequently the higher selectivity towards pyrrolidine.

The product poisoning by *n*-butylamine can not explain the increase of the selectivity to pyrrolidine with the particle size reduction (Fig. 9), since the smaller the particle size, the more open its surface. *N*-butylamine should be bonded more strongly on the smaller nanoparticles, which should result in the decrease of pyrrolidine formation on the smaller nanoparticles. One possible explanation for the size-dependent selectivity is that the surface of the smaller nanoparticle is more oxidized than that of the larger nanoparticle under the same reaction conditions. The relative difference in oxidation state of surface atoms may change the bonding strength difference between the *n*-butylamine and the aromatic species. High oxidation

state of surface atoms may also lower the rate for the more demanding ring-opening process. Thus, the question arises whether there is a significant difference in the oxidation states of the 1-nm and 2-nm nanoparticles under the given reaction condition, a question that can be answered by techniques capable of monitoring oxidation state of catalyst surfaces under reaction conditions.

5.2 Ambient Pressure X-Ray Photoelectron Spectroscopy (AP-XPS)

AP-XPS [45, 46] can be operated at total reactant pressure of up to 10 Torr. The key component making this technique different from the conventional XPS is the differentially pumped electrostatic lens system (Fig. 14) that refocuses the photoelectrons from the sample surface into the object plane of a standard electron energy analyzer working under high-vacuum. The kinetic energy of the photoelectrons can be tuned by varying the energy of the X-ray source. By tuning the kinetic energy of the photoelectrons to an appropriate value, the electron mean free path can be minimized for a given sample surface so that the oxidation state and the composition of the surface layer with the thickness of about 1 nm can be determined.

AP-XPS has been applied to study the oxidation states of Rh nanoparticles with size in the range from 2 to 11 nm during the CO oxidation reaction [47]. It was found that the thickness of surface oxide on the Rh nanoparticles increases with the size reduction, which is correlated with the increase of the turnover.

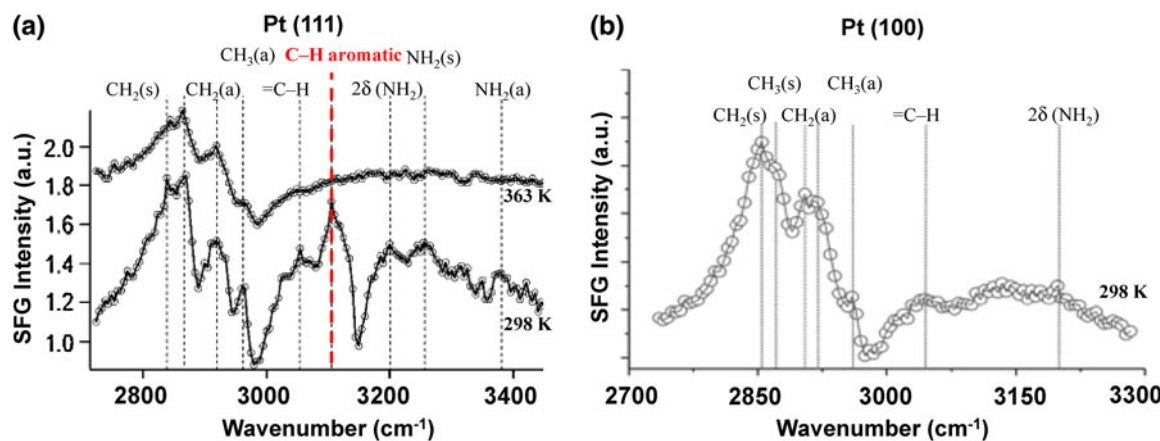
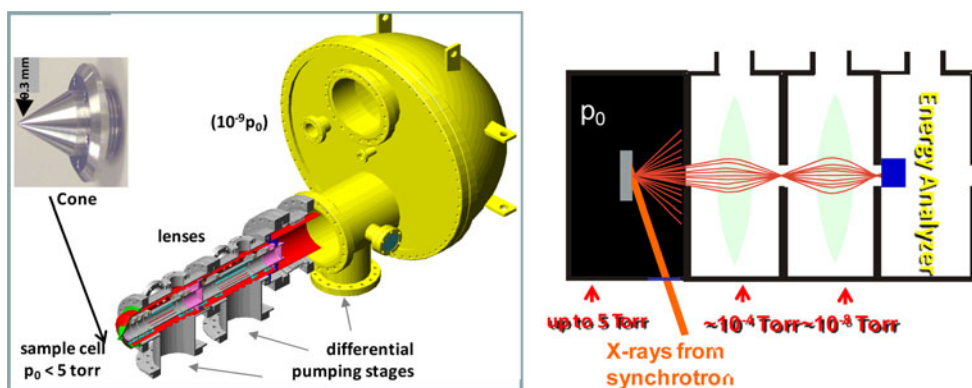


Fig. 13 **a** The SFG spectra of the Pt(111) surface during the pyrrole hydrogenation reaction at 298 and 363 K. **b** The SFG spectrum of the Pt(100) surface during the pyrrole hydrogenation at 298 K. 3 Torr of pyrrole and 30 Torr of hydrogen are used in these studies. Note that

the C–H aromatic peak at 3105 cm^{-1} (the red dashed line) shows up on the Pt(111) surface at 298 K, and is missing on the Pt(111) surface at high temperature (363 K) and on the Pt(100) surface at 298 K

Fig. 14 Cartoons of the photoelectron detector used in ambient pressure X-ray photoelectron spectroscopy (AP-XPS) technique



It is of great importance to determine the surface composition of bimetallic catalysts under the reaction conditions. A recent AP-XPS study [48] of the surface composition of Rh/Pd and Pd/Pt bimetallic nanoparticles demonstrated that the surface composition of nanoparticles are extremely sensitive to their ambient chemical environment. For example, under the oxidizing atmosphere of NO, the Rh atoms are pulled out to the surface of the $\text{Rh}_{0.5}\text{Pd}_{0.5}$ nanoparticles (Fig. 15), while under a reducing mixture of CO and NO, the Pd surface concentration increases. The surface composition variation of a given metal is up to 20% at 300 °C. These results indicate that the concentration of surface active sites on bimetallic catalysts, especially, these in the form of nanoparticles, may change significantly with the reaction conditions. The restructuring phenomenon observed in the bimetallic NPs induced by changes in reactive gas offers an interesting way of engineering the nanostructure of NPs for catalysis and other applications. One goal could be the synthesis of “smart” catalysts whose structure changes advantageously depending on the reaction environment.

5.3 High Pressure Scanning Tunneling Microscopy (HP-STM)

Scanning tunneling microscopy operating under high pressure and high temperature conditions offers a promising way to monitor the structure of surfaces and adsorbates on the molecular level during surface reactions. Since the first system [49] was demonstrated in 1992, several HP-STM systems have been designed and applied to in situ catalytic reaction studies [50–53]. A recently developed system [54] is shown in Fig. 16. By integrating a small high pressure reactor into the UHV chamber, the new system is capable of imaging surfaces at the atomic resolution under a wide range of pressures (from 10^{-13} bar to several bars) and temperatures (from 300 to 700 K).

The HP-STM studies on catalyst surfaces unveiled many phenomena which were not seen under ultrahigh vacuum conditions. For example [49], exposing the Pt(110) surface to hydrogen at low pressures induces missing row reconstruction. High pressure of hydrogen can further roughen the surface (Fig. 17a). The overall surface corrugation is

Fig. 15 The chemical environment effects on the surface segregation of the Rh/Pd and Pd/Pt nanoparticles detected by AP-XPS

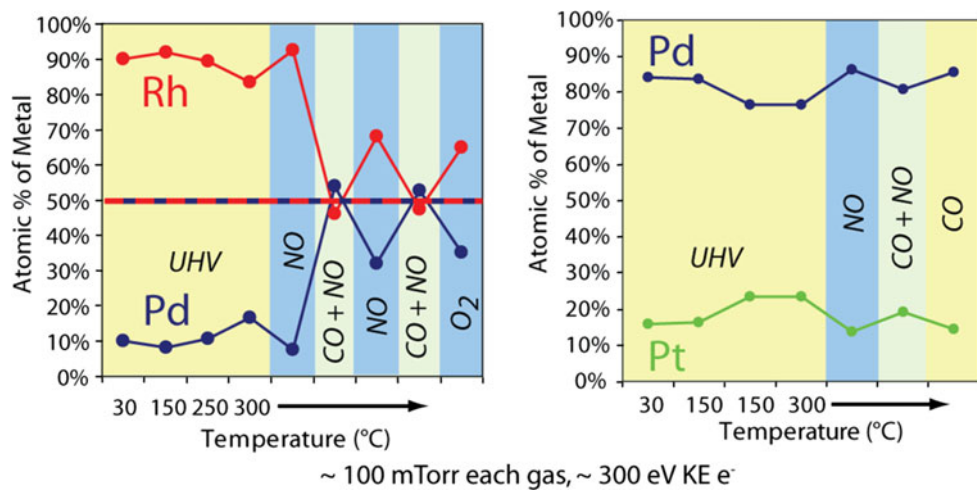
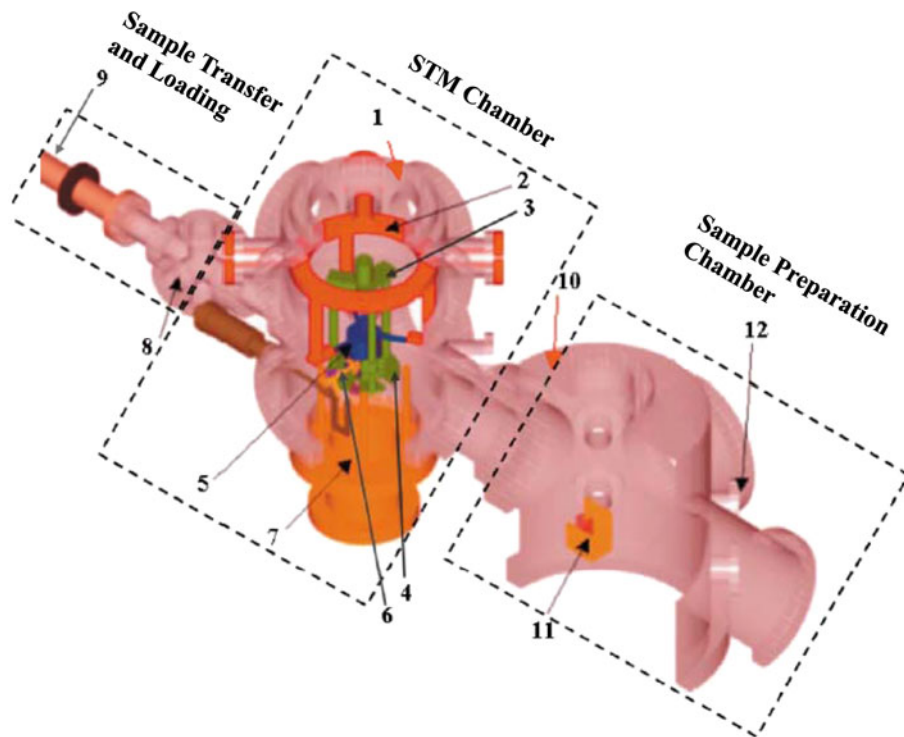


Fig. 16 Cartoon of a recent designed HP-STM experiment system: (1) view window, (2) mounting framework, (3) docking scaffold, (4) docking disk, (5) high pressure reactor (STM body housed within), (6) bayonet seal, (7) guide rod of docking scaffold, (8) sample/tip load-lock system, (9) transfer rod, (10) gate valve, (11) four-finger sample stage, and (12) sputtering ion gun



approximately 1.5 nm after exposing the surface to 1.7 atm. of hydrogen at 425 K for 5 h. These reconstructions are stable in vacuum. Even larger scale structures with the (111) facets are present after the subsequent exposure to 1 atm. of oxygen (Fig. 17b). The periodicities of the hill and valley structure are in the range of 10–30 nm. The overall surface corrugation is greater than 20 nm. A similar roughening effect was also observed under a high pressure of CO (Fig. 17c).

Adsorbate mobility is another important phenomenon observed in the HP-STM studies of hydrocarbon conversion reactions. During the hydrogenation/dehydrogenation

of cyclohexene over the Pt(111) surface, no distinguishable feature of the surface can be resolved by STM (Fig. 18) [55]. Given the limited scanning speed of the STM tip (typically, 10 nm/ms), the featureless STM image implies that the adsorbates move at a speed much higher than that of the STM tip. After poisoning the reaction by a small amount of CO, the reaction turnover stops and ordered structures emerge on the surface since the coadsorption of strongly bonded CO limits the mobility of the hydrocarbon adsorbates. These results and the similar observations during the ethylene hydrogenation [56] suggest that, on the catalyst surfaces saturated by various hydrocarbon

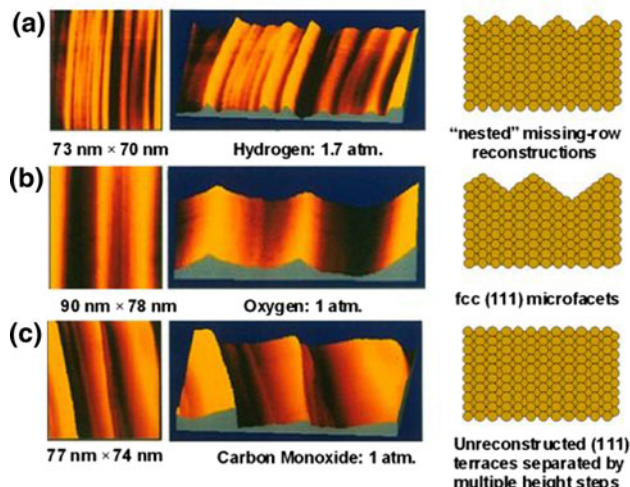


Fig. 17 The surface structure changes induced by the atmospheric pressure of **a** hydrogen, **b** oxygen, and **c** carbon monoxide at 425 K

adsorbates under high pressures, the adsorbate mobility is crucial for the active sites occupied by the inactive species to be continuously released to the reactive species.

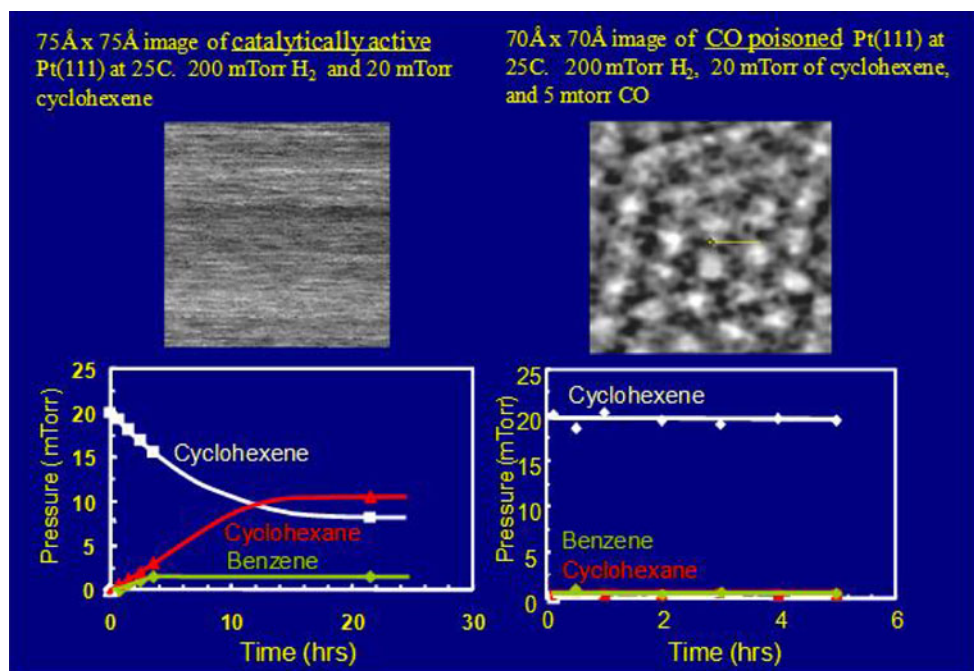
5.4 Catalytic Metal–Semiconductor Nanodiode

The metal catalysts dispersed on the reducible oxide supports usually exhibit enhancement of catalytic activity and selectivity. This effect first observed by Schwab [57] is commonly referred to as strong metal support interaction (SMSI). Figure 19a shows turnover rate and selectivity of CO hydrogenation over several Ni/oxide catalysts [58].

Compared to the Ni catalysts supported on the inert SiO_2 support, the turnover rate of CO hydrogenation is significantly higher over the Ni/TiO₂ catalysts, and the selectivity to the C_{2+} hydrocarbons increases. SMSI effects have also been observed on the catalysts with the inverted structure (see the inset in Fig. 19b). The turnover rate of the CO₂ hydrogenation over TiO₂ on Rh substrate changes with the coverage of TiO₂. The maximum turnover rate occurs at about 50% of a monolayer of oxide coverage. It was proposed by Schwab that the SMSI effect may be due to an electron exchange between support and metal catalyst [59]. This idea was then developed further by Verykios et al., who suspected that the Schottky-like barrier at the metal-oxide interface may be responsible for the formation of the unique electronic structure at the metal-oxide interface [60]. The question is: if there is electron transport at the interface, how can we detect it under reaction conditions?

It turns out that a metal–semiconductor nanodiode shown in Fig. 20a is capable of capturing the electrons transported from metal surface to the semiconductor [61, 62]. The electrons excited during catalytic reaction on the metal surface may travel ballistically through the metal thin film with thickness less than the mean free path of the electron (~ 10 nm for Pt). The ballistic electrons with kinetic energy higher than the Schottky barrier height can enter into the semiconductor (Fig. 20b). These electrons return to the metal thin film through an ammeter connecting the semiconductor and the metal film. In this way, a continuous electric current called chemicurrent can be generated during a catalytic reaction on the metal surface.

Fig. 18 The correlation between the mobility of adsorbates and the reaction turnover rate during the hydrogenation/dehydrogenation of cyclohexene over the Pt(111) surface



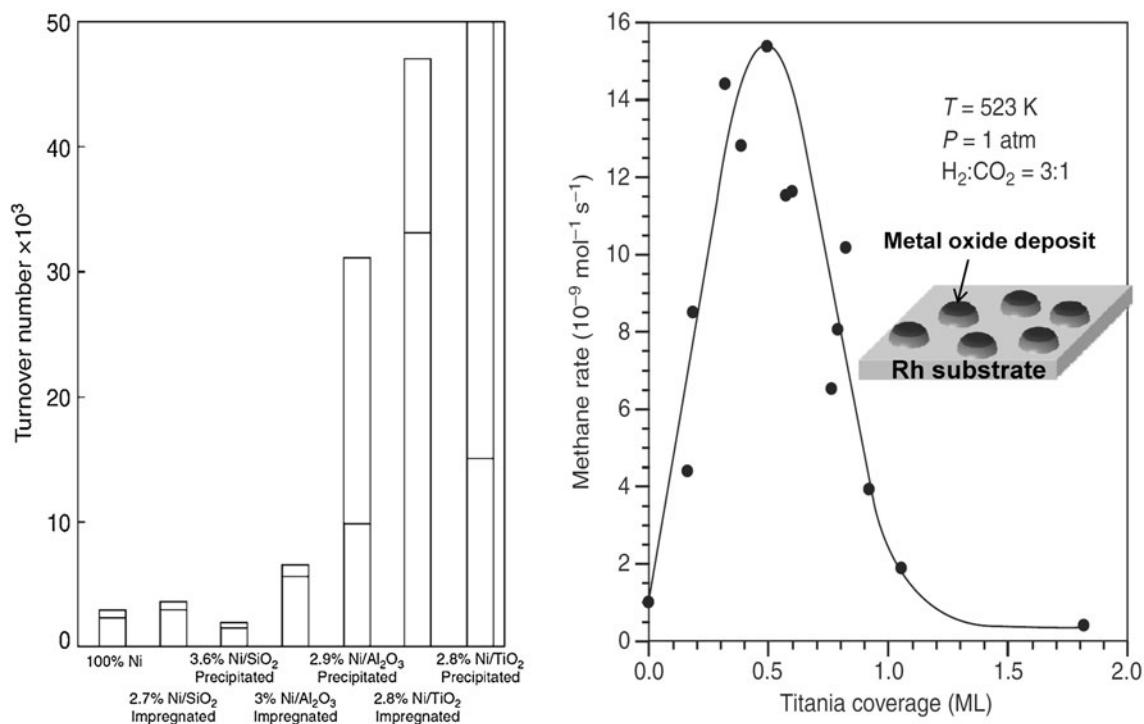
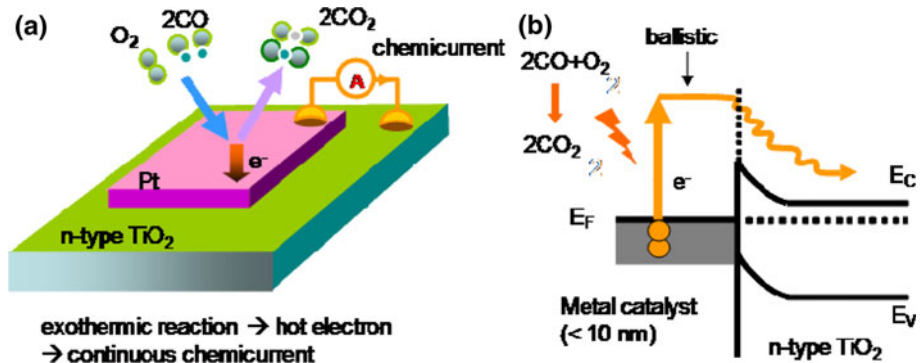


Fig. 19 a The SMSI effects on the reactivity and selectivity of the CO hydrogenation over Pt/oxides catalysts. **b** The oxide coverage dependence of methane formation rate over the inverted rhodium/TiO₂ surfaces (see the inset)

Fig. 20 a Cartoon of the nanodiode detector for measuring the chemicurrent generated by the catalytic reaction on the metal thin film surface. **b** The energy band diagram showing the excitation of electrons in the metal and their transport through the metal thin film in the semiconductor



So far, the chemicurrents have been detected during several catalytic reactions. Figure 21a, b show the measured chemicurrents and the turnover rates for CO oxidation [63] and hydrogen oxidation [64], respectively. The fact that the activation energies for the turnover rate and the chemicurrent are very close to each other in these two cases indicates that the electron transport is induced by the catalytic reaction over the metal surface.

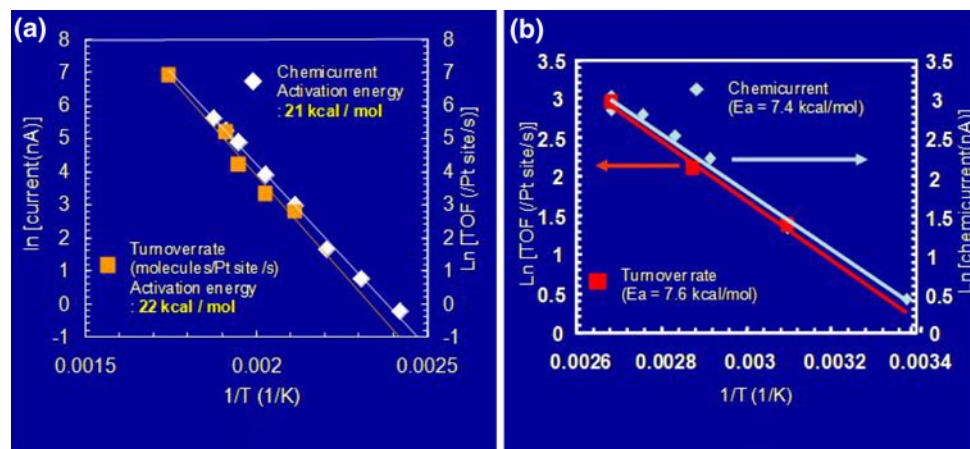
6 Conclusion and Outlook

Achieving the high catalytic selectivity is the goal of catalysis science in 21th century. In this paper, we have shown that the advances in nanotechnology enable us to control the

concentration of the active sites for different reaction products by tuning the size and shape of nanoparticles. The active site for a given product could be a certain atomic arrangement of metal atoms, the surface atom in a certain oxidation state, bimetallic surface site with a specific composition, or the interface between the metal nanoparticle and the oxide support. Under reaction conditions, active sites may reconstruct due to the elevated temperature, or be blocked by strongly adsorbed intermediates. All these complexities make it essential to develop *in situ* techniques, and to identify the active site under reaction conditions.

The development of surface science techniques for studying the molecular factors which control the selectivity of catalytic reactions under practical reaction conditions is of paramount importance to catalysis science in the 21th

Fig. 21 The correlation between the reaction turnover rate and the chemicurrent intensity during **a** CO oxidation, and **b** hydrogen oxidation



century. These molecular factors include: (1) Surface structure (the size and shape of nanoparticles), (2) Surface composition, (3) Adsorbate mobility, (4) Adsorption-induced surface restructuring, (5) Reaction intermediates, (6) Surface oxidation state, and (7) Charge transport at metal/support interfaces.

On the way to design catalysts with 100% selectivity, a number of strategies need to be explored further in the future. The development of hybrid catalysts, which can combine the advantages of heterogeneous, homogeneous, and enzymatic catalysts, is one of the most promising strategies. The merger of homogenous and heterogeneous catalysts can be achieved either by immobilization of homogeneous catalysts onto solid supports or by applying supported heterogeneous catalysts to homogeneous catalytic reactions [8, 65, 66]. The main challenge in this regard is to develop catalyst synthesis approaches that prevent catalyst deactivation due to leaching. Immobilization of enzymatic catalysts, a promising approach to improve enzyme stability, can enable practical uses of enzyme as biocatalyst in fine-chemical and pharmaceutical synthesis [67, 68]. The challenge in the field is again to synthesize the immobilized enzymes with the activity and selectivity comparable to their counterpart in the free form.

Size-controlled sub-nanometer metal clusters of 40 atoms (~ 0.8 nm) or smaller may have unique electronic structures and oxidation states which mimic that of metal ion active sites in homogeneous catalysts. Also, most of the atoms in a sub-nanometer bimetallic cluster are surface atoms, so the surface bimetallic composition is very close to the bulk composition, and will not change significantly by variations in temperature or chemical environment. This stability in surface composition may help us control the active sites on bimetallic catalysts under reaction conditions.

Acknowledgment This work was supported by the Director, Office of Science, Office of Basic Energy Sciences of the U.S. Department of Energy, under Contract DE-A02-05CH11231.

Open Access This article is distributed under the terms of the Creative Commons Attribution Noncommercial License which permits any noncommercial use, distribution, and reproduction in any medium, provided the original author(s) and source are credited.

References

- Berzelius J (1836) *Jahres-Bericht über die Fortschritte der Physischen Wissenschaften*. H. Laupp, Tübingen
- Derouane EG (2001) CaTTech 5:214
- Somorjai GA (1994) *Introduction to surface chemistry and catalysis*. Wiley, New York
- Christensen CH, Norskov JK (2008) *J Chem Phys* 128
- Norskov JK, Bligaard T, Rossmeisl J, Christensen CH (2009) *Nat Chem* 1:37
- Gladysz JA (2001) *Pure Appl Chem* 73:1319
- Gladysz JA (2002) *Chem Rev* 102:3215
- Coperet C, Chabanas M, Saint-Arroman RP, Basset JM (2003) *Angewandte Chemie-Int Ed* 42:156
- Corma A (2004) *Catal Rev Sci Eng* 46:369
- Ertl G, Prigge D, Schloegl R, Weiss M (1983) *J Catal* 79:359
- Yang J, Tschanber V, Habermacher D, Garin F, Gilot P (2008) *Appl Catal B Environ* 83:229
- Somorjai GA, Park JY (2008) *Chem Soc Rev* 37:2155
- Somorjai GA, Park JY (2008) *Angewandte Chemie-Int Ed* 47:9212
- Taylor HS (1925) *Proc R Soc Lond A-Cont Papers Math Phys Character* 108:105
- Somorjai GA, McCrea KR, Zhu J (2002) *Top Catal* 18:157
- Zaera F (2005) *Chem Record* 5:133
- Thomas JM, Thomas WJ (1997) *Principles and practice of heterogeneous catalysis*. VCH, Weinheim; New York
- Somorjai GA (1984) *Surface science view of catalysis: the past, present, and future*. In: *8th international congress on catalysis. Proceedings*, vol 1. Plenary lectures
- Marsh AL, Becroft KA, Somorjai GA (2005) *J Phys Chem B* 109:13619
- Davis SM, Somorjai GA (1980) *J Catal* 65:78
- Strongin DR, Carrazza J, Bare SR, Somorjai GA (1987) *J Catal* 103:213
- Gunter PLJ, Niemantsverdriet JW, Ribeiro FH, Somorjai GA (1997) *Catal Rev Sci Eng* 39:77
- Aiken JD, Finke RG (1999) *J Mol Catal Chem* 145:1
- Narayanan R, El-Sayed MA (2005) *J Phys Chem B* 109:12663
- Somorjai GA, Park JY (2008) *Top Catal* 49:126

26. Zhang YW, Grass ME, Habas SE, Tao F, Zhang TF, Yang PD, Somorjai GA (2007) *J Phys Chem C* 111:12243
27. Lee H, Habas SE, Kweskin S, Butcher D, Somorjai GA, Yang PD (2006) *Angewandte Chemie-Int Ed* 45:7824
28. Park JY, Zhang Y, Grass M, Zhang T, Somorjai GA (2008) *Nano Lett* 8:673
29. Joo SH, Park JY, Tsung CK, Yamada Y, Yang PD, Somorjai GA (2009) *Nat Mater* 8:126
30. Crooks RM, Zhao MQ, Sun L, Chechik V, Yeung LK (2001) *Acc Chem Res* 34:181
31. Peng XH, Pan QM, Rempel GL (2008) *Chem Soc Rev* 37:1619
32. Huang W, Kuhn JN, Tsung CK, Zhang Y, Habas SE, Yang P, Somorjai GA (2008) *Nano Lett* 8:2027
33. Bratlie KM, Lee H, Komvopoulos K, Yang PD, Somorjai GA (2007) *Nano Lett* 7:3097
34. Rioux RM, Hsu BB, Grass ME, Song H, Somorjai GA (2008) *Catal Lett* 126:10
35. Kuhn JN, Huang WY, Tsung CK, Zhang YW, Somorjai GA (2008) *J Am Chem Soc* 130:14026
36. Grass M, Rioux R, Somorjai G (2009) *Catal Lett* 128:1
37. Tsung CK, Kuhn JN, Huang WY, Aliaga C, Hung LI, Somorjai GA, Yang PD (2009) *J Am Chem Soc* 131:5816
38. Kliewer CJ, Somorjai GA (in preparation) Size effect on furan hydrogen over Pt nanoparticles, manuscript
39. Witham CA, Huang W, Tsung C-K, Kuhn JN, Somorjai GA, Toste FD (2009) *Nat Chem.* Accepted
40. Guyot-Sionnest P, Superfine R, Hunt JH, Shen YR (1989) In: Wang ZZ (ed) *Proceedings of the topical meeting on laser materials and laser spectroscopy*. World Scientific Press, Singapore
41. Shen YR (1989) *Nature* 337:519
42. Cremer PS, Su XC, Somorjai GA, Shen YR (1998) *J Mol Catal Chem* 131:225
43. Somorjai GA, Kliewer CJ (2009) *React Kinet Catal Lett* 96:191
44. Kliewer CJ, Bieri M, Somorjai GA (2008) *J Phys Chem C* 112:11373
45. Salmeron M, Schlogl R (2008) *Surf Sci Rep* 63:169
46. Bluhm H, Havecker M, Knop-Gericke A, Kiskinova M, Schlogl R, Salmeron M (2007) *MRS Bull* 32:1022
47. Grass ME, Zhang YW, Butcher DR, Park JY, Li YM, Bluhm H, Bratlie KM, Zhang TF, Somorjai GA (2008) *Angewandte Chemie-Int Ed* 47:8893
48. Tao F, Grass ME, Zhang YW, Butcher DR, Renzas JR, Liu Z, Chung JY, Mun BS, Salmeron M, Somorjai GA (2008) *Science* 322:932
49. McIntyre BJ, Salmeron MB, Somorjai GA (1992) *Catal Lett* 14:263
50. Rasmussen PB, Hendriksen BLM, Zeijlemaker H, Ficke HG, Frenken JWM (1998) *Rev Sci Instrum* 69:3879
51. Petersen L, Schunack M, Schaefer B, Linderoth TR, Rasmussen PB, Sprunger PT, Laegsgaard E, Stensgaard I, Besenbacher F (2001) *Rev Sci Instrum* 72:1438
52. Kolmakov A, Goodman DW (2003) *Rev Sci Instrum* 74:2444
53. Rossler M, Geng P, Wintterlin J (2005) *Rev Sci Instrum* 76
54. Tao F, Tang D, Salmeron M, Somorjai GA (2008) *Rev Sci Instrum* 79
55. Montano M, Salmeron M, Somorjai GA (2006) *Surf Sci* 600:1809
56. Grunes J, Zhu J, Yang MC, Somorjai GA (2003) *Catal Lett* 86:157
57. Schwab GM (1946) *Trans Faraday Soc* 42:689
58. Bartholomew CH, Pannell RB, Butler JL (1980) *J Catal* 65:335
59. Schwab GM, Koller K (1968) *J Am Chem Soc* 90:3078
60. Akubuiro EC, Verykios XE (1988) *J Catal* 113:106
61. Nienhaus H (2002) *Surf Sci Rep* 45:3
62. Ji ZX, Zuppero A, Gidwani JM, Somorjai GA (2005) *Nano Lett* 5:753
63. Park JY, Somorjai GA (2006) *J Vac Sci Technol B* 24:1967
64. Hervier A, Renzas JR, Park JY, Somorjai GA (2009) *Nano Lett* Accepted
65. Astruc D, Lu F, Aranzaes JR (2005) *Angewandte Chemie-Int Ed* 44:7852
66. de Jesus E, Flores JC (2008) *Ind Eng Chem Res* 47:7968
67. Kim J, Grate JW, Wang P (2006) *Chem Eng Sci* 61:1017
68. Lee CH, Lin TS, Mou CY (2009) *Nano Today* 4:165